The transition between steady and oscillatory motion in three-dimensional rotating convection

J. H. P. Dawes

Department of Applied Mathematics and Theoretical Physics, University of Cambridge, Silver Street, Cambridge, CB3 9EW, UK. Tel: +44-1223-337900. Fax: +44-1223-337918. Email: J.H.P.Dawes@damtp.cam.ac.uk

Abstract

We investigate the transition between oscillatory and steady convection at onset in low Prandtl number rotating convection. This is found to be dominated by a three-dimensional mode interaction. We construct the normal form and compute the normal form coefficients at the codimension 2 point directly from the PDEs for Boussinesq rotating convection. The normal form dynamics exhibit irregular bursting behaviour created by a heteroclinic cycle containing points 'at infinity'. The full dynamics in the region of the codimension 2 point are investigated and show the existence of additional quasiperiodic oscillations and further heteroclinic cycles near onset.

Key words: 3D convection, rotation, mode interaction, bursting, heteroclinic cycle

1 Introduction

It is well-known that the onset of convection in a rotating Boussinesq fluid with a low Prandtl number ($\sigma < 0.677$) is oscillatory if the rotation rate is large enough [1]. From linear theory there is a sharp transition between the regions in the (σ, τ) plane where the onset of convection is steady or oscillatory, with a corresponding jump in the critical wavenumber of convection. This transition boundary can be analysed by considering a codimension 2 mode interaction which describes the dynamics at one point on the boundary between the two regions. In fact, as is often the case, the normal form dynamics give a good guide to the observed behaviour in a large neighbourhood of the transition boundary due to the generality of the structure of the normal form and the fact that the ratio of the most unstable wavenumbers for steady and oscillatory convection does not vary greatly along the transition line.

Previous work on steady convection has focussed on the Küppers–Lortz instability [2–4] where (if the rotation rate is large enough) rolls are unstable at the onset of convection to perturbations in the form of rolls aligned at an angle to the original rolls. This angle of instability depends very sensitively on the Prandtl number: in the limit $\sigma \to \infty$ the critical angle is found to be approximately 58°. The use of stress-free boundaries introduces further instabilities of steady rolls, to perturbations aligned at very small angles [5]. These small–angle instabilities are not seen when no–slip boundaries are imposed, and like the Küppers–Lortz instability, can be described dynamically as a heteroclinic cycle connecting rolls at varying orientations.

In the oscillatory regime two-dimensional analyses have shown that either Travelling Rolls or Standing Rolls can be preferred [6]. In three dimensions the possibilities are more complex, and have been investigated only recently [7]. In particular, there is an analogous Küppers–Lortz type of instability for Travelling Rolls which occurs for values of $\sigma < 0.3$.

The outline of the paper is as follows. In section 2 we specify the idealised convection problem considered, derive the normal form equations which govern behaviour near the codimension 2 point and discuss the dynamics of the steady and oscillatory parts of the problem separately. A complete analysis of the dynamics of the mode interaction is presented in section 3. Section 4 contains a discussion and presents conclusions.

2 Rotating convection

Rotating Boussinesq convection is governed by three dimensionless parameters: the Prandtl number $\sigma = \nu/\kappa$ (the ratio of the rates at which velocity and temperature gradients diffuse), the Rayleigh number R which is proportional to the temperature difference across the layer and the square root of the Taylor number $\tau = 2h^2\Omega/\nu$ where h is the depth of the layer, Ω is the rotation rate and ν is the kinematic viscosity.

Let $\mathbf{u} = (u_x, u_y, u_z)$ and θ be perturbations to the conduction solution $\mathbf{u}_0 = 0$, $T_0 = 1 - z$ for the velocity and temperature fields respectively. The evolution of these perturbations is governed by the following non-dimensionalised equations (in the co-rotating frame):

$$(\partial_t - \sigma\nabla^2)\nabla^2\mathbf{u} + \sigma\tau\partial_z\boldsymbol{\omega} + \sigma R\mathbf{D}\,\theta = \nabla \times \nabla \times (\boldsymbol{\omega} \times \mathbf{u}) \tag{1}$$

$$(\partial_z - \nabla^2)\theta - u_z = -\mathbf{u} \cdot \nabla\theta \tag{2}$$

$$\nabla \cdot \mathbf{u} = 0 \tag{3}$$

where the double curl of the momentum equation has been taken (to eliminate the pressure term), $\boldsymbol{\omega} = \nabla \times \mathbf{u}$ and the vector operator $\mathbf{D} \equiv (\partial^2_{xz}, \partial^2_{yz}, -\partial^2_{xx} - \partial^2_{yy})$ We impose periodic boundaries in the horizontal directions and stress-free, fixed temperature upper and lower boundaries.

$$\partial_z u_x = \partial_z u_y = u_z = \theta = 0 \qquad \text{at} \quad z = 0, 1 \tag{4}$$

From a linear stability analysis of the conduction (trivial) solution (see, for example Chandrasekhar [1]) the critical Rayleigh number for the onset of steady convection at wavenumber α_s is

$$R_s = \frac{(\alpha_s^2 + \pi^2)^3 + \pi^2 \tau^2}{\alpha_s^2} \tag{5}$$

and, when $\sigma < 0.677$ and $\tau > \tau_c(\sigma)$ the transition to steady convection is preceeded by a Hopf bifurcation from the trivial solution. The critical Rayleigh number for the onset of oscillatory convection at wavenumber α_o is found to be

$$R_o = \frac{2\sigma^2 \pi^2 \tau^2}{\alpha_o^2 (1 + \sigma)} + \frac{2(\alpha_o^2 + \pi^2)^3 (\sigma + 1)}{\alpha_o^2} \tag{6}$$

The frequency of the Hopf bifurcation at onset is given by

$$\omega_0^2 = (\alpha_o^2 + \pi^2)^2 \sigma^2 \left[\frac{\tau^2 \pi^2 (1 - \sigma)}{(\alpha_o^2 + \pi^2)^3 (1 + \sigma)} - 1 \right] \tag{7}$$

The line marked ℓ_1 in figure 1 separates regions of the (σ, τ)-plane where steady or oscillatory convection is preferred at onset; the line is defined by the condition that the critical Rayleigh numbers for steady and oscillatory convection are equal. We restict attention to wavenumbers α_s and α_o which minimise R_s and R_o respectively as in an extended layer we expect to see convection cells with these horizontal scales.

As we cross line ℓ_1 in figure 1, the preferred horizontal wavenumber jumps, because $\alpha_s \neq \alpha_o$ in general, during what must somehow be a smooth transition from steady to oscillatory behaviour. We can explain this transition fully in the neighbourhood of the codimension 2 point where the ratio of critical wavenumbers $\alpha_s / \alpha_o = \sqrt{2}$ by fitting the marginal modes for steady convection onto a square lattice (which is required to keep the centre manifold of the bifurcation problem finite dimensional), see figure 2(a). To locate this $1 : \sqrt{2}$ resonance we have to satisfy the following four conditions:

$$\frac{dR_s}{d(\alpha_s^2)} = 0 \quad \Rightarrow \quad 2(\alpha_s^2+\pi^2)^3 - 3\pi^2(\alpha_s^2+\pi^2)^2 - \pi^2\tau^2 = 0 \tag{8}$$

$$\frac{dR_o}{d(\alpha_o^2)} = 0 \quad \Rightarrow \quad 2(\alpha_o^2+\pi^2)^3 - 3\pi^2(\alpha_o^2+\pi^2)^2 - \frac{\sigma^2\pi^2\tau^2}{(1+\sigma)^2} = 0 \tag{9}$$

$$R_s = R_o \quad \Rightarrow \quad \frac{2(1+\sigma)(\pi^2+\alpha_o^2)^3}{\alpha_o^2} + \frac{2\sigma^2\pi^2\tau^2}{\alpha_o^2(1+\sigma)} = \frac{(\alpha_s^2+\pi^2)^3+\pi^2\tau^2}{\alpha_s^2} \tag{10}$$

$$\alpha_s = \alpha_o\sqrt{2} \tag{11}$$

These conditions are satisfied at parameter values $\sigma_c = 0.61288$, $\tau_c = 332.22$ and $R_c = R_s = R_o = 22661$ giving a critical steady wavenumber $\alpha_s = 8.7773$. This point is marked P on figure 1. The dashed line in figure 1 shows the result of satisfying conditions (8), (9) and (11) simultaneously. This illustrates how close the ratio $s = \alpha_s/\alpha_o$ stays to $\sqrt{2}$ along ℓ_1. This is also demonstrated in figure 2(b).

2.1 The normal form

By imposing a square lattice we reduce the symmetry group of the problem from the non-compact special Euclidean group $SE(2)$ of rotations and translations of the plane to the compact group $\mathbb{Z}_4 \ltimes T^2$. This ensures the existence of a finite dimensional centre manifold for the bifurcation problem and enables us to derive a set of ODEs (amplitude equations) for the dynamics. The form of the amplitude equations can be determined purely from symmetry considerations. The role of the governing fluid equations is to determine the numerical values of the coefficients in the normal form.

We impose a square planform so that the vertical velocity is represented as a sum of four travelling waves in the $\pm x$ and $\pm y$ directions and two steady modes along the diagonals of the square lattice, see figure 2(a).

$$\begin{aligned} u_z(x,y,z,t) = Re(&A_1 e^{i(\alpha x-\omega t)} + A_2 e^{-i(\alpha x+\omega t)} + B_1 e^{i(\alpha y-\omega t)} \\ &+B_2 e^{-i(\alpha y+\omega t)} + C e^{i\alpha(x+y)} + D e^{i\alpha(x-y)}) f(z) \end{aligned} \tag{12}$$

where $f(z)$ represents the vertical structure of the velocity field. The amplitude equations describing the evolution of $A_1, \ldots, D$ on a slower timescale must be equivariant under the group $\mathbb{Z}_4 \ltimes T^2$ generated by quarter-turn rotations about the z-axis and translations in the x and y directions:

$$\rho : (x,y) \to (y,-x) : \quad (A_1, A_2, B_1, B_2, C, D) \to (B_1, B_2, A_2, A_1, \bar{D}, C) \tag{13}$$

$$\theta_{\xi,\eta} : (x,y) \to (x+\xi/\alpha, y+\eta/\alpha)$$
$$(A_1,A_2,B_1,B_2,C,D) \to (A_1e^{i\xi}, A_2e^{-i\xi}, B_1e^{i\eta}, B_2e^{-i\eta}, Ce^{i(\xi+\eta)}, De^{i(\xi-\eta)}) \quad (14)$$

We also impose the Boussinesq symmetry:

$$m_z : z \to 1-z : \quad (A_1,A_2,B_1,B_2,C,D) \to -(A_1,A_2,B_1,B_2,C,D) \quad (15)$$

These equivariance conditions lead to the following amplitude equations on the centre manifold (truncated at third order):

$$\begin{aligned}\dot{A}_1 = {} & A_1[\hat{\mu}_1 + a|A_1|^2 + b|A_2|^2 + c|B_1|^2 + d|B_2|^2 + \lambda_1|C|^2 + \lambda_2|D|^2] \\ & + e\bar{A}_2B_1B_2 + \lambda_3A_2CD \end{aligned} \quad (16)$$

$$\begin{aligned}\dot{A}_2 = {} & A_2[\hat{\mu}_1 + a|A_2|^2 + b|A_1|^2 + c|B_1|^2 + d|B_2|^2 + \lambda_1|C|^2 + \lambda_2|D|^2] \\ & + e\bar{A}_1B_1B_2 + \lambda_3A_1\bar{C}\bar{D} \end{aligned} \quad (17)$$

$$\begin{aligned}\dot{B}_1 = {} & B_1[\hat{\mu}_1 + a|B_1|^2 + b|B_2|^2 + c|A_2|^2 + d|A_1|^2 + \lambda_1|D|^2 + \lambda_2|C|^2] \\ & + e\bar{B}_2A_1A_2 + \lambda_3B_2C\bar{D} \end{aligned} \quad (18)$$

$$\begin{aligned}\dot{B}_2 = {} & B_2[\hat{\mu}_1 + a|B_2|^2 + b|B_1|^2 + c|A_1|^2 + d|A_2|^2 + \lambda_1|D|^2 + \lambda_2|C|^2] \\ & + e\bar{B}_1A_1A_2 + \lambda_3B_1\bar{C}D \end{aligned} \quad (19)$$

$$\begin{aligned}\dot{C} = {} & C[\mu_2 + \beta_1|C|^2 + \beta_2|D|^2 + \beta_3|A_1|^2 + \bar{\beta}_3|A_2|^2 + \beta_4|B_1|^2 + \bar{\beta}_4|B_2|^2] \\ & + \nu_1B_1\bar{B}_2D + \nu_2A_1\bar{A}_2\bar{D} \end{aligned} \quad (20)$$

$$\begin{aligned}\dot{D} = {} & D[\mu_2 + \beta_1|D|^2 + \beta_2|C|^2 + \beta_3|B_2|^2 + \bar{\beta}_3|B_1|^2 + \beta_4|A_1|^2 + \bar{\beta}_4|A_2|^2] \\ & + \nu_1A_1\bar{A}_2\bar{C} + \nu_2\bar{B}_1B_2C \end{aligned} \quad (21)$$

As usual for problems involving Hopf bifurcations in normal form there is also a normal form symmetry which corresponds to a time translation. This generates an additional S^1 group:

$$\theta_\phi : t \to t + \phi/\omega_0 \quad (A_1,A_2,B_1,B_2,C,D) \to (A_1e^{-i\phi}, A_2e^{-i\phi}, B_1e^{-i\phi}, B_2e^{-i\phi}, C, D)$$

Hence the complete symmetry group of the problem is $\Gamma = \mathbb{Z}_4 \ltimes T^2 \times S^1$. The third-order truncation is generically found to be sufficient to determine the dynamics near codimension 2 bifurcation points such as this. The coefficients $\mu_2, \beta_1, \beta_2, \nu_1$ and ν_2 are forced to be real by symmetry, but all other coefficients are, in general, complex. We write $\hat{\mu}_1 = \mu_1 + i\tilde{\omega}(\mu_1)$ where μ_1 and $\tilde{\omega}$ are both real.

When $C = D = 0$ the equations reduce to the normal form for a Hopf bifurcation with $\mathbb{Z}_4 \ltimes T^2$ symmetry. This has been studied in detail by Knobloch and Silber [8] and is summarised in section 2.2. When $A_1 = A_2 = B_1 = B_2 = 0$ the equations for C and D describe the usual steady bifurcation to either roll or square solutions, discussed in section 2.3.

2.2 The Hopf bifurcation

We recall the definitions of an isotropy subgroup $\Sigma_{\mathbf{x}} = \{\gamma \in \Gamma : \gamma\mathbf{x} = \mathbf{x}\}$ and a fixed point subspace $\mathrm{Fix}(\Sigma) = \{\mathbf{x} : \gamma\mathbf{x} = \mathbf{x} \ \ \forall\ \gamma \in \Sigma\}$. The Hopf bifurcation with $\mathbb{Z}_4 \ltimes T^2$ symmetry generically produces four branches with two dimensional fixed point subspaces [8], which therefore exist for all values of the normal form coefficients by the Equivariant Hopf Theorem [9]. These are denoted Travelling Rolls (TR), Standing Rolls (SR), Standing Squares (SS) and Alternating Rolls (AR). A further periodic solution, Standing Cross Rolls (SCR), exists for some combinations of normal form coefficients - its existence is not guaranteed by the Equivariant Hopf Theorem since it has a four dimensional fixed point subspace. The stability properties of these periodic orbits depend on the values of the normal form coefficients a - e and are summarised in table 1. Table 1 also contains a quasiperiodic solution, the Travelling Bimodal (TB) branch. This solution also has a four dimensional fixed point subspace and so is not guaranteed to appear for all coefficient values [8]. We expect that further doubly and triply-periodic solutions can exist in regions of parameter space, as when $c = d$ the quasiperiodic solutions found in [10] will exist.

The Travelling Roll periodic orbit is an example of a *relative equilibrium*, it is a periodic orbit where time evolution around the orbit is equivalent to the action of a spatial symmetry: for a point $\mathbf{u_0}$ on the orbit, $\phi_t(\mathbf{u_0}) = \gamma_t\mathbf{u_0}$ for some spatial translation γ_t which depends on t. For the Travelling Roll solution any time advance is equivalent to a suitable spatial translation: this implies the existence of a continuous group orbit of TR solutions. None of the other four periodic solutions is a relative equilibrium.

Just as for the Hopf bifurcation with $D_4 \ltimes T^2$ symmetry, there exist open regions of the parameter space where none of the branches with two dimensional fixed point subspaces are stable. Unlike the $D_4 \ltimes T^2$ - symmetric case, a further possibility for the dynamics is the formation of a structurally stable heteroclinic cycle connecting four Travelling Roll states. This is not possible in the $D_4 \ltimes T^2$ - symmetric case as the reflection symmetries ensure that the stability of a TR orbit to perturbations at 90° clockwise to it is the same as its stability to perturbations at 90° anticlockwise.

2.3 The steady bifurcation

When $A_1 = A_2 = B_1 = B_2 = 0$ the phases of C and D decouple from equations from their moduli. Applying the equivariant branching lemma we can guarantee that two branches of solutions bifurcate when $\mu_2 = 0$. These are of the form $C \neq 0$, $D = 0$, denoted rolls, and $C = D \neq 0$, denoted squares. When the normal form coefficients are non-degenerate (the non-degeneracy conditions are that a finite number of combinations of the coefficients do not vanish) the third order truncation fully describes the dynamics and these are all the solutions that appear. When both bifurcate supercritically, exactly one of them is stable, and when one or both bifurcate subcritically, neither can be stable.

2.4 Calculation of the normal form coefficients

We calculate the normal form coefficients in (16) - (21) using modified perturbation theory, expanding the Rayleigh number R and square root of the Taylor number τ in powers of ε in addition to the velocity and temperature fields:

$$\mathbf{u} = \varepsilon \mathbf{u}_1 + \varepsilon^2 \mathbf{u}_2 + \dots \tag{22}$$
$$\theta = \varepsilon \theta_1 + \varepsilon^2 \theta_2 + \dots \tag{23}$$
$$R = R_c + \varepsilon R_1 + \varepsilon^2 R_2 + \dots \tag{24}$$
$$\tau = \tau_c + \varepsilon \tau_1 + \varepsilon^2 \tau_2 + \dots \tag{25}$$

The numerical values of R_c and τ_c give the location of the $1 : \sqrt{2}$ point located in section 2. We then equate the terms in (1) - (2) in each power of ε. This leads to the following schematic equations:

$$\mathcal{O}(\varepsilon): \quad \mathcal{L}(\mathbf{u}_1, \theta_1) = 0 \tag{26}$$
$$\mathcal{O}(\varepsilon^2): \quad \mathcal{L}(\mathbf{u}_2, \theta_2) = \mathcal{N}_1(\mathbf{u}_1, \theta_1) \tag{27}$$
$$\mathcal{O}(\varepsilon^3): \quad \mathcal{L}(\mathbf{u}_3, \theta_3) = \mathcal{N}_2(\mathbf{u}_1, \theta_1, \mathbf{u}_2, \theta_2) \tag{28}$$

where $\mathcal{L}$ is the linear operator on the LHS of equations (1) - (2) and $\mathcal{N}_1$ and $\mathcal{N}_2$ represent nonlinear terms.

By taking stress-free, fixed temperature boundary conditions (4) the solution can be expressed completely and simply in terms of exponentials; the linear operator has exponentials as eigenfunctions. We use the incompressibility condition (3) as an independent check that the calculation is correct at each order. It would be possible to use a poloidal-toroidal decomposition, but the

existence of mean flow terms means they would have to be explicitly added into the scheme. At second order in ε in the calculation we apply the solvability condition to find that $R_1 = T_1 = 0$. At third order the values of the normal form coefficients are derived and the modes $A_1, \ldots, D$ evolve on a slow timescale $t' = \varepsilon^2 t$. We will drop the prime from now on, and denote the slow timescale simply by t.

The bifurcation parameters μ_1 and μ_2 are linearly related by the modified perturbation expansion to R_2 and τ_2:

$$\begin{pmatrix} \mu_1 + i\tilde{\omega} \\ \mu_2 \end{pmatrix} = \begin{pmatrix} 1.493 + 2.451i & -0.1184 - 0.3745i \\ 6.441 & -0.5482 \end{pmatrix} \begin{pmatrix} R_2/1000 \\ \tau_2 \end{pmatrix} \tag{29}$$

The form of this transformation agrees with intuition: increasing R_2 will increase both bifurcation parameters, and increasing τ_2 will decrease them. The subsequent analysis of equations (16) - (21) explains the transition from steady to oscillatory motion near the $1 : \sqrt{2}$ point P.

3 $1 : \sqrt{2}$ resonance in rotating convection

3.1 Bifurcations from the trivial solution

The trivial (conduction) solution is stable in the quadrant $(\mu_1 < 0, \mu_2 < 0)$. It loses stability in a Hopf bifurcation when $\mu_1 = 0$, $\mu_2 < 0$ and in a steady-state bifurcation when $\mu_1 < 0$, $\mu_2 = 0$. By rescaling the amplitudes $A_1 = \hat{A}_1\sqrt{\mu_1}, \ldots, C = \hat{C}\sqrt{\mu_2}$ etc we see that the bifurcation parameters μ_1 and μ_2 only enter the rescaled equations in the combination μ_1/μ_2: all bifurcations occur on straight lines through the origin. The bifurcation diagram can be most easily presented by defining $\theta = \tan^{-1}(\mu_2/\mu_1)$ and following a path of increasing θ, $-\pi/2 \leq \theta \leq \pi$. The Hopf bifurcation occurs at $\theta = -\pi/2$ and the steady-state one at $\theta = \pi$. The full bifurcation diagram is shown in figure 3.

At $\theta = -\pi/2$ the trivial solution loses stability to the four oscillatory modes A_1, A_2, B_1 and B_2; this is the Hopf bifurcation with $\mathbb{Z}_4 \ltimes T^2$ symmmetry analysed in section 2.2: all four periodic solution branches bifurcate supercritically, and the Travelling Roll branch is stable, as shown in figure 1. The stability of the TR solution $|A_1|^2 = -\mu_1/a_r$, $A_2 = B_1 = B_2 = 0$ to perturbations in the C and D modes is given by the linearisation of (16) - (21) around the TR solution:

$$\dot{C} = C\left(\mu_2 - \frac{\beta_3\mu_1}{a_r}\right) \qquad \dot{D} = D\left(\mu_2 - \frac{\beta_4\mu_1}{a_r}\right) \tag{30}$$

where sub or superscripts r and i denote the real and imaginary parts of a coefficient. Using the numerically calculated values of the coefficients, the TR solution is stable in the region $-\pi/2 < \theta < \tan^{-1}\beta_3^r/a_r = -1.5266$ where it loses stability in a *subcritical* pitchfork bifurcation which creates solutions with (for example) A_1 and C both non-zero. These unstable solutions are denoted *Travelling Rolls plus Diagonal Rolls* (TR+DR):

$$|A_1|^2 = \frac{\mu_1\beta_1 - \mu_2\lambda_1^r}{\lambda_1^r\beta_3^r - a_r\beta_1} \qquad |C|^2 = \frac{a_r\mu_2 - \beta_3^r\mu_1}{\lambda_1^r\beta_3^r - a_r\beta_1} \tag{31}$$

3.2 Bursting behaviour

Numerical investigations of the normal form above this bifurcation point show irregular "bursts" of activity (see figure 4): trajectories approach the unstable TR orbit and follow its unstable manifold out to large amplitudes before being re-injected to the neighbourhood of a Standing Rolls (SR) orbit in the invariant subspace $\mathcal{S}_1 = \{(A_1, A_2, 0, 0, 0, 0)\}$. The SR orbit is, for this region of θ, stable to perturbations in the C and D modes, but it is unstable to the TR orbit within $\mathcal{S}_1$ so points close to the SR orbit move towards the TR orbit staying close to the subspace $\mathcal{S}$. Near the TR orbit they follow the unstable manifold of the TR orbit and perturbations in the C-direction grow rapidly. In the invariant subspace $\mathcal{S}_2 = \{(A_1, 0, 0, 0, C, 0)\}$ the unstable manifold of the TR orbit extends to infinity for $\tan^{-1}\beta_3^r/a_r = -1.5266 < \theta < \pi/2$, i.e. commencing at the subcritical pitchfork bifurcation. Trajectories close to this subspace reach very large amplitudes before being attracted back towards the SR orbit and the subspace $\mathcal{S}_1$, causing the cycle to repeat. This is illustrated schematically in figure 5.

The existence of a structurally stable connection between the TR orbit and a point at infinity enables the dynamics to exhibit bursts of finite duration, but unbounded amplitude. Bursts with these properties have been observed in experiments on (non-rotating) binary fluid convection [11] and a dynamical explanation for the experimental observations involving a system of two oscillatory modes with weakly broken D_4 symmetry is discussed in [12, section 3]. This nearly D_4-symmetric system also contains a structurally stable connection to a point at infinity and the mechanism for the generation of bursts is formally very similar. The major differences between the two examples are that the equations (16) - (21) are exactly $\mathbb{Z}_4 \ltimes T^2$-symmetric and involve an interaction between steady and oscillatory modes. There is also no convenient coordinate transformation to study the dynamics in the invariant subspace 'at

infinity' for (16) - (21) analytically, as there is for [12].

The dynamics within the $\mathcal{S}_2$ subspace can be analysed by restricting equations (16) - (21) to $\mathcal{S}_2$:

$$\dot{A} = A_1[\hat{\mu}_1 + a|A_1|^2 + \lambda_1|C|^2] \tag{32}$$
$$\dot{C} = C[\mu_2 + \beta_1|C|^2 + \beta_3|A_1|^2] \tag{33}$$

To determine the behaviour as $|A|$ and $|C|$ become large, we write $A_1 = Re^{i\theta_1}\cos\eta$ and $C = Re^{i\theta_2}\sin\eta$. We also rescale time by a factor of R^2. The new time variable is $T = R^2 t$. The evolution equations for R, η, θ_1 and θ_2 are

$$\frac{dR}{dT} = \frac{1}{R}(\mu_1\cos^2\eta + \mu_2\sin^2\eta) + R[a_r\cos^4\eta + (\lambda_1^r + \beta_3^r)\cos^2\eta\sin^2\eta + \beta_1\sin^4\eta] \tag{34}$$
$$\frac{d\eta}{dT} = \frac{\cos\eta\sin\eta(\mu_2 - \mu_1)}{R^2} + \cos\eta\sin\eta[(\beta_1 - \lambda_1^r)\sin^2\eta + (\beta_3^r - a_r)\cos^2\eta] \tag{35}$$
$$\frac{d\theta_1}{dT} = \frac{\tilde{\omega}}{R^2} + a_i\cos^2\eta + \lambda_1^i\sin^2\eta \tag{36}$$
$$\frac{d\theta_2}{dT} = \beta_3^i\cos^2\eta \tag{37}$$

From (35) we can see that as $R \to \infty$ (in a finite time),

$$\eta \to \eta^* = \tan^{-1}\left(\frac{a_r - \beta_3^r}{\beta_1 - \lambda_1^r}\right)^{1/2} \simeq 0.91829 \tag{38}$$

and θ_1 and θ_2 evolve at constant rates, say $\phi_1 \equiv a_i\cos^2\eta^* + \lambda_1^i\sin^2\eta^*$ and $\phi_2 \equiv \beta_3^i\cos^2\eta^*$, in the limit of large R. The bifurcation parameters $\hat{\mu}_1$ and μ_2 do not play a role in the dynamics at large R so they may be ignored. The stability of the $\mathcal{S}_2$ subspace to perturbations in the A_2 and D modes can now be investigated by linearising equations (17) and (21) about the large-R solution for A_1 and C. Using the scaled time variable T, and neglecting the (small) linear terms, we obtain:

$$R^2\frac{dA_2}{dT} = A_2[b|A_1|^2 + \lambda_1|C|^2] + \lambda_3\bar{D}R^2e^{i(\phi_1-\phi_2)T}\cos\eta^*\sin\eta^* \tag{39}$$
$$R^2\frac{d\bar{D}}{dT} = \bar{D}[\beta_2|C|^2 + \bar{\beta}_4|A_1|^2] + \nu_1A_2R^2e^{-i(\phi_1-\phi_2)T}\cos\eta^*\sin\eta^* \tag{40}$$

where the complex conjugate of the D equation has been taken. We can now perform a change of variables to eliminate the exponentials on the RHS of (39) - (40). Writing

$$A_2 = \hat{A}_2 e^{i(\phi_1-\phi_2)T/2} \qquad \text{and} \qquad \bar{D} = \hat{D} e^{-i(\phi_1-\phi_2)T/2} \tag{41}$$

we drop the carats on $\hat{A}_2$ and $\hat{D}$ and substitute for $|A_1|^2$ and $|C|^2$ to obtain

$$\frac{dA_2}{dT} = A_2 \left[(b - \frac{i}{2}a_i + \frac{i}{2}\beta_3^i)\cos^2\eta^* + (\lambda_1^r + \frac{i}{2}\lambda_1^i)\sin^2\eta^* \right] + \lambda_3 D \cos\eta^* \sin\eta^* \tag{42}$$

$$\frac{dD}{dT} = D \left[(\bar{\beta}_4 + \frac{i}{2}a_i - \frac{i}{2}\beta_3^i)\cos^2\eta^* + (\beta_2 + \frac{i}{2}\lambda_1^i)\sin^2\eta^* \right] + \nu_1 A_2 \cos\eta^* \sin\eta^* \tag{43}$$

The eigenvalues of this (complex) linearisation are in two complex conjugate pairs. One pair has a negative real part, and one pair has a positive real part indicating instability to perturbations transverse to $\mathcal{S}_2$.

The nonlinear development of the instability can most easily be analysed by returning to the full equations (16) - (21), performing the time rescaling $T = R^2 t$ and ignoring the linear terms as before. The time rescaling effectively means the trajectory spends much more time at large amplitudes, enabling the dynamics at large R to be found by numerical integration. The results of such an integration are shown in figure 6 and show a stable quasiperiodic trajectory on which $|A_1| = |A_2|$ and R is decreasing. From equation (34) for dR/dT, for example, we can derive an equation for $Q = 1/R$. The equation for Q is

$$\frac{dQ}{dT} = -Q^3(\mu_1\cos^2\eta + \mu_2\sin^2\eta) - Q[a_r\cos^4\eta + (\lambda_1^r + \beta_3^r)\cos^2\eta\sin^2\eta + \beta_1\sin^4\eta] \tag{44}$$

which shows that the equations governing the dynamics near infinity have an invariant subspace $Q = 0$. (The same is true if we define $R^2 = |A_1|^2 + |A_2|^2 + |C|^2 + |D|^2$ and $Q = 1/R$). This flow-invariance enables us to propose that there is a structurally stable connection between the intersection of $\mathcal{S}_2$ and $Q = 0$ and the quasiperiodic solution in $Q = 0$. While the intersection of $\mathcal{S}_2$ and $Q = 0$ is stable in $\mathcal{S}_2$ and unstable in $Q = 0$, the quasiperiodic solution is stable within $Q = 0$ and unstable to transverse perturbations. This gives rise to the spiralling behaviour as the trajectory returns from a large amplitude excursion close to the invariant subspace $Q = 0$. On such a trajectory we find that as R decreases so do $|C|$ and $|D|$ and the trajectory spirals in towards the SR solution in $\mathcal{S}_1$ to repeat the cycle.

The re-injection mechanism (trajectories from infinity being attracted towards the SR orbit) is due to the collision of a 3-torus with the SR orbit: as θ increases further, numerical integrations show that a 3-torus moves away from the SR orbit, gains stability, and the bursting ceases. This global bifurcation can best be described as a boundary crisis of the 3-torus, and occurs at approximately $\theta = -1.41$.

3.3 Bifurcation structure for larger θ

At larger values of θ the 3-torus, which lies in the invariant subspace $B_1 = B_2 = 0$, undergoes a reverse Hopf bifurcation into a stable quasiperiodic orbit. numerical investigations indicate that this bifurcation occurs at $\theta \simeq -1.20$. As θ increases further, this quasiperiodic orbit (seen as a periodic orbit in modulus/argument co-ordinates) approaches the Diagonal Roll fixed point at $|C|^2 = -\mu_2/\beta_1$. At $\theta = 1.7126$ the quasiperiodic orbit becomes part of a stable heteroclinic cycle connecting the two Diagonal Roll states ($|C|^2 = -\mu_2/\beta_1, D = 0$) and ($C = 0, |D|^2 = -\mu_2/\beta_1$).

The stability of this robust cycle can be analytically determined from the linearisation about the DR fixed point ($|C|^2 = -\mu_2/\beta_1, D = 0$). The linearisation has eigenvalues with real parts $\mu_1 - \mu_2\lambda_1^r/\beta_1$ in the A_1 and A_2 directions, and eigenvalues with real parts $\mu_1 - \mu_2\lambda_2^r/\beta_1$ in the B_1 and B_2 directions. When $\mu_1 - \mu_2\lambda_1^r/\beta_1 > 0$ and $\mu_1 - \mu_2\lambda_2^r/\beta_1 < 0$, the DR solution is unstable with respect to perturbations in the A_i modes, and stable with respect to perturbations in the B_i modes. The flow-invariant subspaces $\mathcal{S}_3 = \{(0, 0, B_1, B_2, C, D)\}$ and $\mathcal{S}_4 = \{(A_1, A_2, 0, 0, C, D)\}$ are related by the quarter-turn rotation symmetry ρ which exchanges the two DR fixed points. The DR cycle is asymptotically stable if eigenvalues transverse to the cycle have negative real parts (45a), and if the ratio of the real parts of the eigenvalues in the stable and unstable directions is greater than one (45b). This leads to the following conditions

$$\beta_2 - \beta_1 < 0 \qquad \frac{|\mu_1 - \mu_2\lambda_2^r/\beta_1|}{\mu_1 - \mu_2\lambda_1^r/\beta_1} > 1 \tag{45}$$

This last condition on the ratio of the real parts of the eigenvalues holds for $\theta > 1.7126 = \tan^{-1} 2\beta_1/(\lambda_1^r + \lambda_2^r)$. At this value of θ, then, the cycle undergoes a resonant heteroclinic bifurcation. This global bifurcation is similar to that seen in the $2:1$ steady-state mode interaction investigated by Proctor and Jones [13]. The cycle is stable until $\theta = 2.2727$ at which point the DR fixed point gains stability in a subcritical pitchfork bifurcation with the *Travelling Rolls plus Diagonal Rolls* solution which was mentioned earlier. The DR solution is stable for $2.2727 < \theta < \pi$: $\theta = \pi$ is the location of the steady-state bifurcation from the origin. This bifurcation sequence is summarised in figure 3.

3.4 Bursting behaviour along ℓ_1

The behaviour found in the region of the codimension 2 point P extends over a wide range of the (σ, τ) plane, and explains the general features of the transition above the point where the lines ℓ_1 and ℓ_2 meet in figure 1. Below this

point the Hopf bifurcation produces stable SR solutions, not TR, and we would not expect the dynamics to resemble those near P. Numerical integrations of the governing PDEs (1) - (3) using the code of Cox and Matthews [14] have indicated a sequence of periodic, bursting and then triply-periodic dynamics in agreement with the normal form behaviour, over the region between the two black squares on figure 1 (see figure 7). We expect that the dynamics for Taylor numbers larger than τ_c (i.e. above P in figure 1) are very similar, but at these high values of τ the numerical experiments become more difficult and time-consuming to perform.

4 Discussion and conclusions

We have analysed a properly three-dimensional interaction between steady and oscillatory modes of convection which involves the most unstable wavenumbers selected at the onset of convection. As such we expect the dynamics of the resulting ODEs to be relevant to understanding the fluid dynamics near onset. The analysis, although complete in itself, has several limitations. Most importantly the theory does not allow for the analysis of the stability of the dynamics near the $1:\sqrt{2}$ point to modes at varying angles. We have also not discussed long wavelength modulational instabilities that may arise.

The results presented here would have to be modified if the Boussinesq symmetry of the normal form was absent: then the normal form for the mode interaction would contain quadratic terms combining steady and oscillatory modes. These might greatly alter the dynamics (see [15] for example).

We expect the $1:\sqrt{2}$ normal form to describe the transition from oscillatory to steady convection over a large part of ℓ_1 since the ratio of critical wavenumbers α_s/α_o varies only very little as σ increases along ℓ_1, see figure 2(b). For ratios of wavenumbers close to $1:\sqrt{2}$ we can rigorously derive amplitude equations on the centre manifold which have the same structure as (16)-(21) because, for nearby wavenumber ratios, there are only T^2-equivariant terms at cubic order which are equivalent to those used to construct the $1:\sqrt{2}$ normal form. This is perhaps unexpected, as the $1:\sqrt{2}$ resonance is the only possible mode interaction using the 'fundamental representations' for both steady and oscillatory modes: each gives only 4 points on the critical circle of wavevectors. For nearby wavenumber ratios we will have to consider either 4 oscillatory and 4 steady modes or 8 oscillatory and 2 steady modes to fully describe the mode interaction. This will be studied in more detail in a future paper.

The subcritical bifurcations in the normal form dynamics coupled with the lack of reflection symmetries gives rise to bursting and robust heteroclinic cycling dynamics. The overall bifurcation diagram is very different to the se-

quence of symmetry-breaking bifurcations seen in the magnetoconvective case [15]. The mechanism for the appearance of bursting behaviour in the $1:\sqrt{2}$ mode interaction involves both a boundary crisis of a torus, where it collides with a periodic orbit which has stable and unstable manifolds, and a structurally stable connection from the periodic orbit to infinity contained within an invariant subspace. Without the invariant subspace such a boundary crisis would lead to bursts with only a *finite* amplitude. However, the existence of the heteroclinic connection to infinity within an invariant subspace allows the bursting in the normal form an unbounded range although the exact amplitudes achieved will be sensitive to numerical and experimental noise. The generation of bursting dynamics by heteroclinic connections to infinity has been observed in other contexts [12].

Unlike the small-angle instabilities mentioned in the introduction, this $1:\sqrt{2}$ mode interaction will persist when no-slip boundaries instead of stress-free ones are used. Due to the shift of ℓ_1 to larger values of τ, the $1:\sqrt{2}$ point occurs at a substantially lower value of σ, with τ changing little. From the results of [4] we can estimate the position of the resonance as $(\sigma,\tau) \simeq (0.17, 300)$. The dynamics on either side of ℓ_1 at this point are very different: for lower σ, Standing Rolls are preferred over Travelling Rolls and in the region of steady convection the initial bifurcation to rolls is subcritical instead of supercritical. Nevertheless, the normal form equations (16) - (21) are still valid and the new values of the coefficients can be calculated by a modified perturbation expansion. The results of [4] also indicate that the ratio of critical wavenumbers does not very greatly along ℓ_1 in the case of no-slip boundaries, so the resulting dynamics should be seen over a similarly wide range of the line dividing regions of steady and oscillatory motion.

It would be interesting to conduct experiments at the relevant parameter values to verify the dynamics analysed in this paper. Experiments on convection in mercury ($\sigma \simeq 0.025$) suffer from the fact that flow visualisation is very difficult. Experiments with mixtures of pressurised, cooled gases are easier to perform, and Prandtl numbers as low as 0.16 can be easily obtained [16].

Acknowledgements

I have benefited from discussions with Michael Proctor and Alastair Rucklidge. I would like to thank Steve Cox and Paul Matthews for making their code for rotating Boussinesq convection available [14]. This work was funded by the EPSRC.

References

[1] S. Chandrasekhar, *Hydrodynamic and Hydromagnetic Stability.* Oxford University Press (1961), republished by Dover Publications, Inc. (1981)

[2] G. Küppers and D. Lortz, Transition from laminar convection to thermal turbulence in a rotating fluid layer. *J. Fluid Mech.* **35** 609–620 (1969)

[3] F.H. Busse and K.E. Heikes, Convection in a rotating layer. *Science* **208** 173–175 (1980)

[4] T. Clune and E. Knobloch, Pattern selection in rotating convection with experimental boundary conditions. *Phys. Rev. E* **47** 2536–2550 (1993)

[5] S.M. Cox and P.C. Matthews, Instabilities of rotating convection. *submitted to J. Fluid Mech.* (1999)

[6] E. Knobloch and M. Silber, Travelling wave convection in a rotating layer. *Geophys. Astrophys. Fluid Dynamics.* **51** 195–209 (1990)

[7] J.H.P. Dawes, Pattern selection in oscillatory rotating convection. *submitted to Physica D.*

[8] E. Knobloch and M. Silber, Hopf Bifurcation with $\mathbb{Z}_4 \times T^2$ Symmetry. *Int. Series of Numer. Math.* **104** 241–252 (1992)

[9] M. Golubitsky, I.N. Stewart and D.G. Schaeffer, *Singularities and Groups in Bifurcation Theory. Volume II.* Springer, Applied Mathematical Sciences Series **69** (1988).

[10] J.H.P. Dawes, Stable quasiperiodic solutions in the Hopf bifurcation with $D_4 \ltimes T^2$ symmetry. *Physics Letters A* **262** 158–165 (1999)

[11] T.S. Sullivan and G. Ahlers, Nonperiodic time dependence at the onset of convection in a binary fluid mixture. *Phys. Rev. A* **38** 3143-3146 (1988)

[12] E. Knobloch and J. Moehlis, Burst mechanisms in hydrodynamics. in *Nonlinear Instability, Chaos and Turbulence. Volume II* eds L. Debnath and D. Riahi. Series: Advances in Fluid Mechanics, Computational Mechanics Publications, Southampton, UK. (1999)

[13] M.R.E. Proctor and C.A. Jones, The interaction of two spatially resonant patterns in thermal convection. Part 1: Exact 1:2 resonance. *J. Fluid Mech.* **188**, 301–335 (1988)

[14] S.M. Cox and P.C. Matthews, A pseudospectral code for convection with an analytic / numerical implementation of horizontal boundary conditions. *Int. J. Numer. Meth. Fluids* **25** 151–166 (1997)

[15] J.H.P. Dawes, The $1 : \sqrt{2}$ Hopf/steady-state mode interaction in three-dimensional magnetoconvection. *Physica* D **139**, 109–136 (2000)

[16] G. Ahlers and K.M.S. Bajaj, Rayleigh-Bénard Convection with Rotation at Small Prandtl Numbers, *Proceedings of the IMA Workshop on 'Pattern Formation in Continuous and Coupled Systems'* eds M. Golubitsky, D. Luss, and S. Strogatz. Springer, (1999)

Table 1
Solution branches in the Hopf bifurcation with $\mathbb{Z}_4 \ltimes T^2$ symmetry, fixed point subspaces and isotropy subgroups. Stability criteria are only given for the first four solutions which are those guaranteed to exist by the Equivariant Hopf Theorem. The symmetry elements are specified as $\rho^n[(\theta_\xi, \theta_\eta), \theta_\phi]$. A solution is stable when all quantities in the last column are negative. $f = a + b - c - d$ and a subscript r denotes 'the real part of'.

Name	Fix(Σ) (A_1, A_2, B_1, B_2)	Σ	Generators of Σ	Stability
TR	$(\mathbf{z}, 0, 0, 0)$	$S^1 \times SO(2)$	$[(\phi, \phi), \phi]$, $[(0, \phi), 0]$	a_r, $b_r - a_r$, $c_r - a_r$, $d_r - a_r$
SR	$(\mathbf{z}, \mathbf{z}, 0, 0)$	$SO(2) \times \mathbb{Z}_2$	$[(0, \phi), 0]$, ρ^2	$a_r + b_r$, $a_r - b_r$, $-f_r$, $\lvert e\rvert^2 - \lvert f\rvert^2$
SS	$(\mathbf{z}, \mathbf{z}, \mathbf{z}, \mathbf{z})$	$\mathbb{Z}_4$	ρ	$a_r + b_r + c_r + d_r + e_r$, $a_r - b_r - e_r$ $f_r - 3e_r$, $Re(f\bar{e}) - \lvert e\rvert^2$
AR	$(\mathbf{z}, \mathbf{z}, i\mathbf{z}, i\mathbf{z})$	$\tilde{\mathbb{Z}}_4$	$\rho[(0, \pi), \pi/2]$	$a_r + b_r + c_r + d_r - e_r$, $a_r - b_r + e_r$ $f_r + 3e_r$, $-Re(f\bar{e}) - \lvert e\rvert^2$
SCR	$(\mathbf{z}_1, \mathbf{z}_1, \mathbf{z}_2, \mathbf{z}_2)$	$\mathbb{Z}_2$	ρ^2	
TB	$(\mathbf{z}_1, 0, \mathbf{z}_2, 0)$	S^1	$[(\phi, \phi), \phi]$	

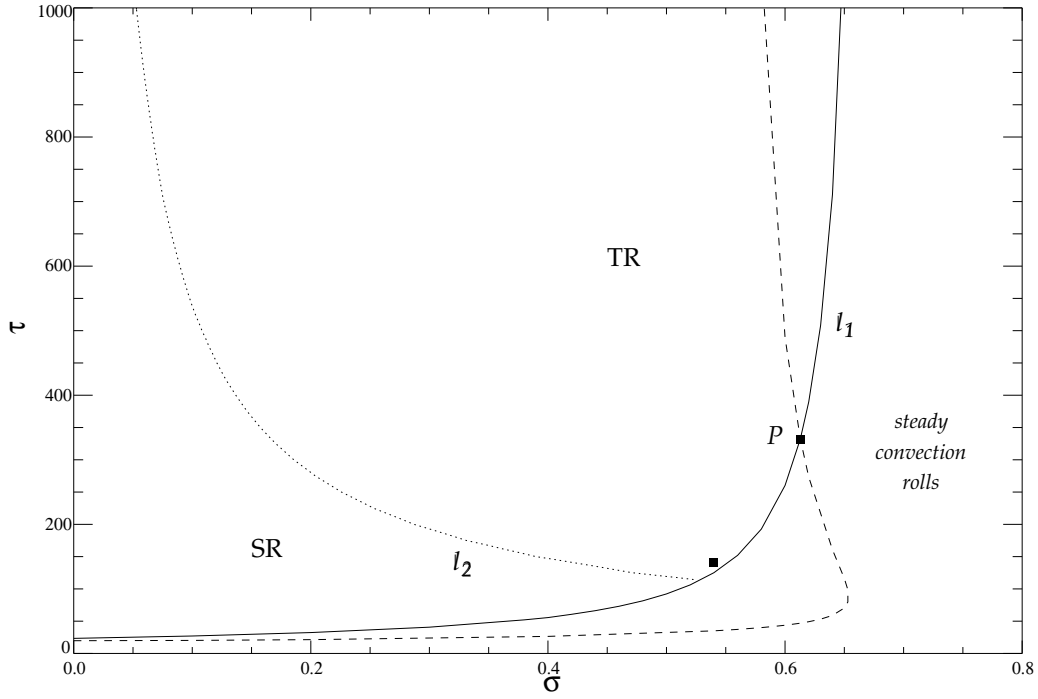

Fig. 1. The line ℓ_1 separates regions of steady and oscillatory convection: steady convection occurs to the right of ℓ_1. The dashed line indicates where the ratio of critical wavenumbers is exactly $1 : \sqrt{2}$. The point P where these two lines cross defines the $1 : \sqrt{2}$ point. The dotted line ℓ_2 divides the regions of stability of Travelling Rolls (TR) and Standing Rolls (SR) near ℓ_1; different planforms are stable for lower σ [7].

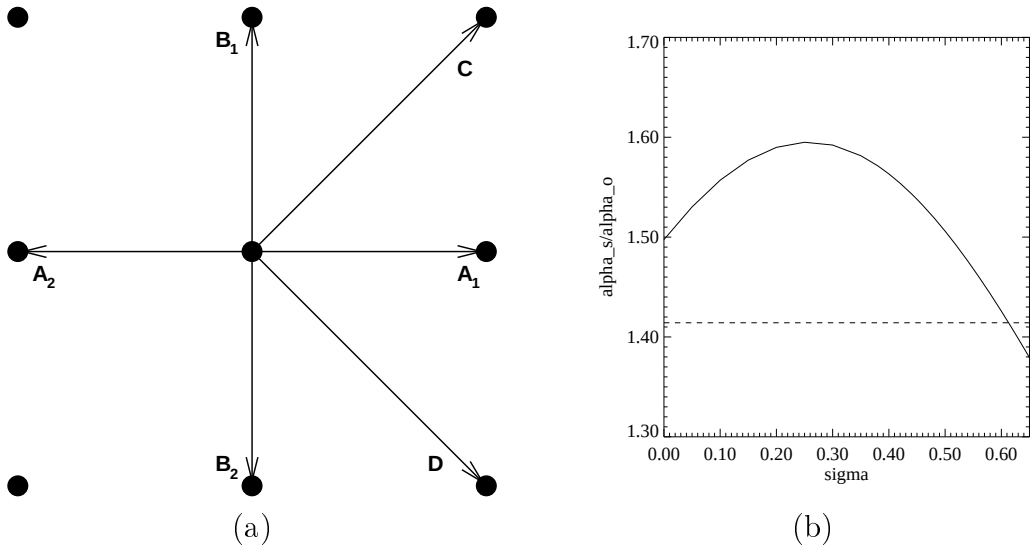

Fig. 2. (a) The geometry of the square planform for the $\mathbb{Z}_4 \ltimes T^2$ mode interaction. A_1, A_2, B_1 and B_2 are the oscillatory modes; C and D are the steady modes. (b) The variation in the ratio of critical wavenumbers α_s/α_o along line ℓ_1 where $R_s = R_o$. The dashed line indicates the ratio $\sqrt{2}$.

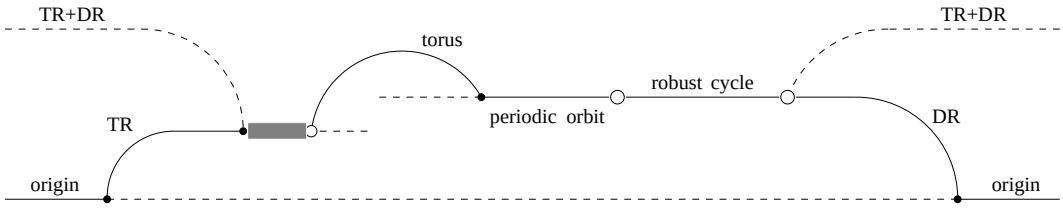

Fig. 3. Bifurcation diagram as θ increases (from left to right) anticlockwise around the origin. Stable solutions are represented by solid lines, unstable solutions by dashed lines. Global bifurcations are shown as open circles, and local bifurcations by filled circles. The shaded region represents the interval of bursting behaviour.

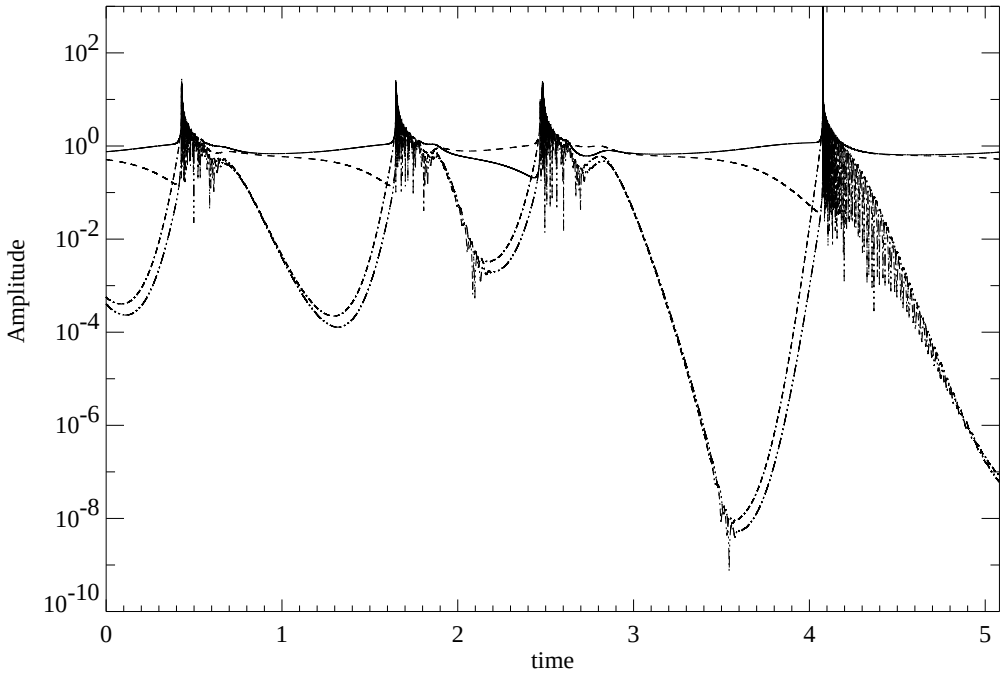

Fig. 4. The time evolution of $|A_1|$ (solid line), $|A_2|$ (dashed), $|C|$ (dash-dash-dotted) and $|D|$ (dash-dot-dotted) for $\theta = -1.46$ showing a trajectory close to the heteroclinic cycle exhibiting irregular bursting behaviour.

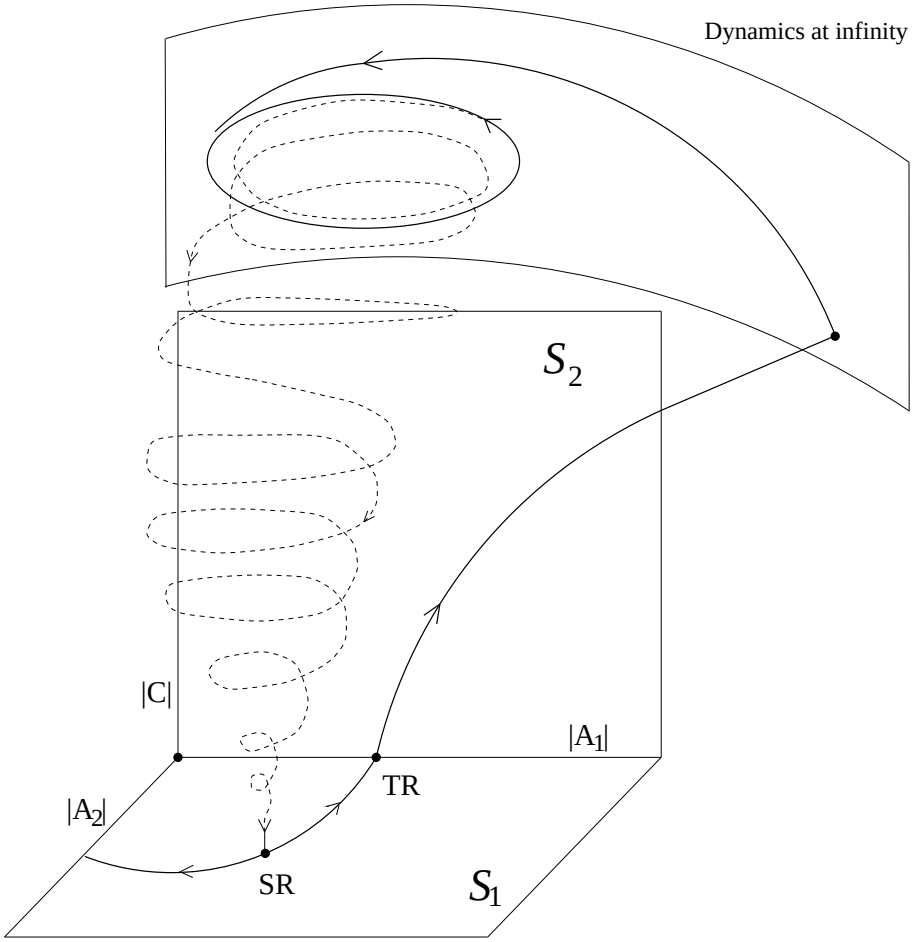

Fig. 5. Schematic representation of the subspaces $\mathcal{S}_1$ and $\mathcal{S}_2$, the heteroclinic connection to infinity and the large amplitude quasiperiodic oscillations which make up one cycle of the bursting behaviour. The thick lines show heteroclinic connections within $\mathcal{S}_1$, $\mathcal{S}_2$ and the invariant subspace at infinity. The dashed trajectory indicates the unstable manifold of the quasiperiodic solution at infinity; it spirals in towards the SR fixed point.

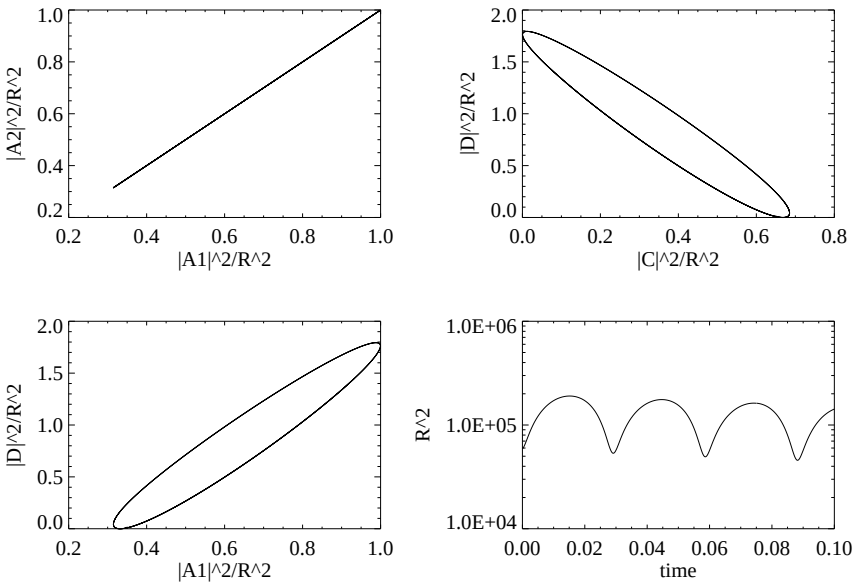

Fig. 6. Quasiperiodic oscillations at large amplitude, a solution trajectory of (16) - (21) after the time rescaling, and ignoring the linear terms.

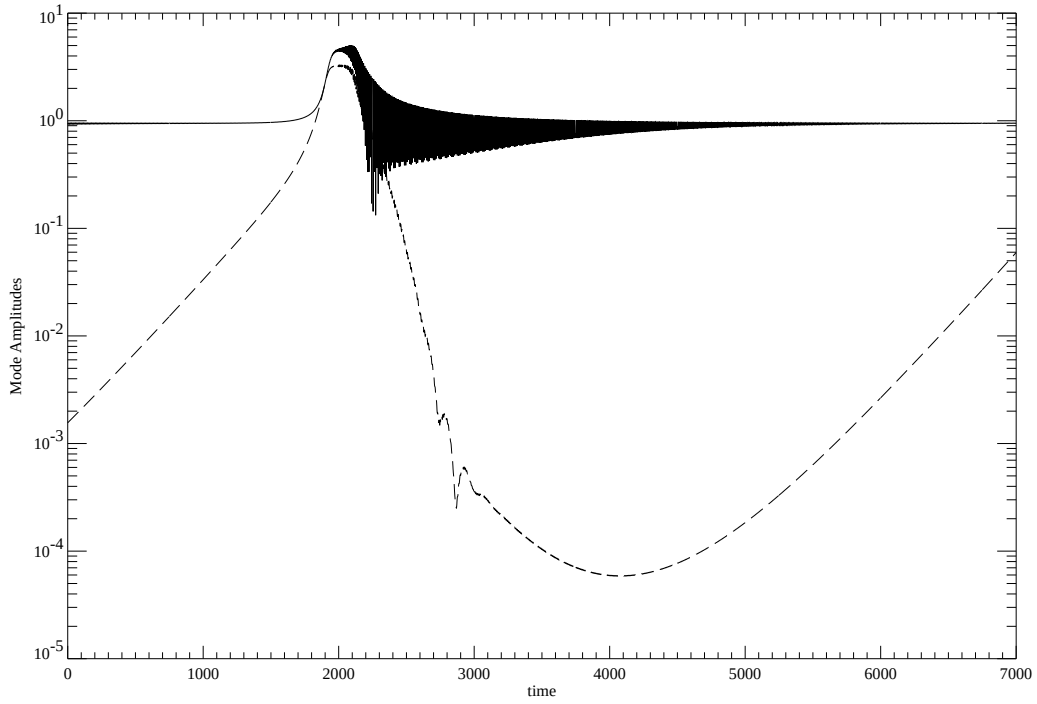

Fig. 7. Bursting seen in numerical integrations of the full PDEs (1) - (3). The solid line gives the amplitude of modes in the $\pm x$ direction (corresponding to $|A_1| + |A_2|$) and the dashed line gives the amplitude of the mode in the $x = y$ direction, representing $|C|$. Intervals where the solid line is constant correspond to Travelling Rolls while the fast oscillations show the approach to the Standing Roll orbit. The physical parameters are $R = 19720$, $\tau = 300$ and $\sigma = 0.6$. Bursting behaviour has been located numerically throughout the region between the two black squares on figure 1.